Available online at www.sciencedirect.com
ScienceDirect
International Journal of Heat and Fluid Flow 29 (2008) 479–494
International Journal of HEAT AND FLUID FLOW
www.elsevier.com/locate/ijhff

# Experimental investigation of a circular radially deforming cylinder near wake using an infrared technique

L. Menfoukh [a], S. Hanchi [a,*], H. Oualli [a], A. Bouabdellah [b], R. Askovic [c]

[a] LMDF Ecole Militaire polytechnique (EMP), Bordj el Bahri, Alger, Algeria
[b] LSTE Université des Sciences et de la technologie (USTHB), Alger, Algeria
[c] LME, UVHC, 59313 Valenciennes Cedex 9, France

Received 28 December 2006; received in revised form 9 October 2007; accepted 12 November 2007
Available online 21 December 2007

**Abstract**

The present experimental study aims at developing a method to control the circular cylinder near wake by radial deformation and understand the underlying physics. Using an infra-red camera, we examine the temperature distribution of the near wake center line of a sinusoidal law radially deforming circular cylinder. From these measurements, the near wake is characterized by the length of the recirculation zone, the vortex formation zone length, the temperature fluctuation maximum intensity and the vortex street shedding frequency. For several deformations frequencies, we study the radial deformation influence on the near wake characteristics. It is noted that the wake structure is strongly affected by the deformation frequency. Among other things, we note the recirculation zone length reduction and the vortex formation zone length reduction when the radial vibrations are close to the "Lock-in" fundamental range. It is also noted that the variations of the vortex shedding frequency depend on the deformation frequency.


*Keywords:* Thermography; Flow control; Lock-in

## 1. Introduction

The flow development around a circular cylinder is a conventional fluid mechanics problem. In spite of the geometry simplicity, the mechanisms implied within the various areas around the cylinder are complex and create a physical phenomenology, difficult to apprehend. Since at least a hundred years, studies have been carried out, trying to understand the mechanisms brought into play. The work of Blasius (1908) (theoretical studies based on the boundary layer principle) and Collins and Dennis (1973), the near wake visualization in transient quasi-established state of Coutenceau and Bouard (1977), and the experimental results of Bearman (1969) and Zdravkovich (1996) on the wall influence in the case of a fixed cylinder, are only some examples among the many studies available in the literature.

In the moving cylinder case, Thom (1933) is one of the pioneers who have followed the flow pattern evolution using visualization, by considering an oscillatory cylinder vibration. Griffin and Votaw (1972) concluded that, when the cylinder vibrates transversely, the shedding frequency adjusts to the forcing vibration. Eddy formation length and the Von-Karman Street longitudinal distance are also influenced by the oscillation frequency.

In numerical simulations, the calculation methods have undergone a rapid evolution in terms of stability and convergence since the works of Thom (1933), Tomotika and Aoi (1950) and Payne (1958).

After the 1970s, the stationary problem being largely understood, researchers set a new objective, the study of the non-stationary Navier–Stokes equations. Using a fourth order finite difference scheme for the Poisson's equation and a second order scheme for the vorticity equation,

* Corresponding author. Tel.: +213 21 86 46 78; fax: +213 21 86 32 04.
*E-mail address:* samir_hanchi@yahoo.fr (S. Hanchi).

0142-727X/$ - see front matter © 2007 Elsevier Inc. All rights reserved.
doi:10.1016/j.ijheatfluidflow.2007.11.001

**Nomenclature**

| | |
|---|---|
| $a$ | variable cylinder radius (m) |
| $a_0$ | initial cylinder radius (m) |
| $D$ | distance between the object and the camera (m) |
| $F_0$ | natural shedding frequency (Hz) |
| $F_d$ | cylinder deformation frequency (Hz) |
| $K$ | wave number vector |
| $L'$ | luminance seen by the camera |
| $N$ | rotational velocity of the engine (rpm) |
| $Re$ | Reynolds number |
| $S(K)$ | wave number spectrum |
| $St$ | Strouhal number |
| $t$ | time (s) |
| $U_{atm}$ | theoretical camera output voltage for a blackbody of temperature $T_{atm}$ according to the calibration (V) |
| $U_{obj}$ | calculated camera output voltage for a blackbody of temperature $T_{obj}$ (V) |
| $U_{ref}$ | theoretical camera output voltage for a blackbody of temperature $T_{ref}$ according to the calibration (V) |
| $U_{tot}$ | measured camera output voltage for the $U_{tot}$ actual case (V) |
| $w$ | $z$-velocity (m/s) |
| $W$ | received radiation power from a blackbody source |
| $\varepsilon$ | emissivity |
| $\varepsilon_{dissV}$ | viscous dissipation |
| $\varepsilon_{dissT}$ | dissipation of temperature fluctuation |
| $\eta$ | Kolmogorov length scale (m) |
| $\kappa$ | thermal diffusivity |
| $v$ | Kolmogorov velocity scale (m/s) |
| $\tau$ | transmissivity |

Ta Phuoc (1980) gave preliminary results for $Re = 1000$. Later, they extended the study to $Re = 9500$ (Ta Phuoc and Bouard, 1985). Through a high resolution simulation based on the vortex method, Koumoutsakos and Leonard (1995) proposed an identification of the mechanisms by which the near wake affects the drag coefficient. For the first time they reached a negative value for the drag coefficient in the case of an abruptly stopped circular cylinder. They suggested the possibility of controlling this flow via the "bulk flow", which gives rise to the secondary vortices, by fluid injection or suction through the cylinder surface. Following this work, Hanchi (1998) numerically investigated control of the "bulk flow" via sinusoidal variation of the cylinder cross-section and its effects on the drag.

The "Lock-in" phenomenon (capture of the shedding frequency by the disturbance frequency), due to the forced (or a self-induced) oscillation of a cylinder placed in a flow, was studied intensively during the last decades (Sarpkaya, 1979; Griffin, 1995; Carberry et al., 2003; Govardhan and Williamson, 2001; Krishnamoorthy et al., 2001). However, the "Lock-in", or the synchronization between the wake shedding and the oscillation frequencies, can also take place when a cylinder oscillates at the same frequency as the fluid flow (Griffin and Ramberg, 1976) and (Ongoren and Rockwell, 1988). Similarly, the "Lock-in" can also be observed when the cylinder is stationary and the fluid flow has an imposed periodic component (Barbi et al., 1986; Armstrong et al., 1986; Hall and Griffin, 1993).

It was shown that the fundamental "Lock-in" is accompanied by a certain number of modifications in the body forces and in the wake structure. Barbi et al. (1986) noted that the average drag force intensity and the lift fluctuations increase in the fundamental "Lock-in" range as compared to those of the non-disturbed flow. Their results agree with the experiments of Tanida et al. (1973). They noted that the average drag and the lift fluctuations of a synchronized oscillating cylinder reach maximum values in the vicinity of the "Lock-in" range center, when the oscillations frequency is close to twice the non-forced frequency. The effects quoted above are associated with near wake cylinder structure modifications. Armstrong et al. (1987) found the same result in the "Lock-in" range center. The force due to the detached vortex power increased by 29% and the vortex formation length decreased from 1.2 to 0.9 of the cylinder diameter. This result is in contradiction with the numerical results of Hall and Griffin (1993) concerning the disturbed flow wake at $Re = 200$. Indeed, they found an increase of the vortex formation length. This contradiction could be attributed to differences in the mechanisms of vortex formation and shedding in the case of low Reynolds numbers ($Re < 350$) and in the case of relatively higher Reynolds numbers ($Re > 350$) (Gerrard, 1966; Green and Gerrard, 1993; Griffin, 1995). The previous results suggest that flow disturbances or equivalent cylinder oscillations can have different effects according to the Reynolds number. Griffin and Ramberg (1976) noted that in the fluid flow "Lock-in" range the Von-Karman Street wavelength increases when the cylinder oscillation frequency decreases. The calculations of Hall and Griffin (1993) show that the disturbed cylinder wake has the same behavior as the wake of a cylinder placed in a disturbed flow.

Oualli et al. (2004) studied effect of a radial deformations combined with a rotation of the circular cylinder on the near wake evolution. Through structural feature visualizations, their experimental observations allowed the qualitative description of the flow. The visualization showed that the pulsation movement reduces the near wake dimensions and delays boundary layer separation angle. Oualli et al. (2004) compared their experimental results with the

numerical results obtained by Hanchi (1998) for the same control parameters (Reynolds number, frequency and amplitude of deformation). There was good agreement between observation and simulation.

The objective of the present study is to show the circular cylinder radial deformation influence on the near wake characteristics by using a particular experimental technique. Indeed, using a smoke generator, we inject a hot fluid within the ambient fluid flow. The resulting temperature gradient is convected by vortices developed behind the cylinder. The mean and the fluctuating temperature fields are examined using an infra-red camera. The measurements showed that the wake is characterized by the recirculation area length, the vortex formation length, the maximum fluctuation intensity, the developed vortex radius and the vortex shedding frequencies.

## 2. Theory

### 2.1. Analogy between the spectrum of temperature fluctuation and the spectrum of turbulence inertial subrange

Let the wave number spectrum, $S(K)$, represent turbulent kinetic energy as a function of the wave number vector $K$. If the turbulence is isotropic, then the spectrum is independent of the orientation of the wave number vector and depends on its magnitude $K$ only. In that case we can write

$$\overline{u^2} = \int_0^\infty S(K)\mathrm{d}K. \tag{1}$$

We will derive the form of $S(K)$ for a range of wave numbers in which the turbulence is nearly isotropic.

Let's associate a wave number $K$ with an eddy of size $K^{-1}$. Small eddies are represented by large wave numbers. Suppose $l$ is the scale of the large eddies. At the relatively small scales represented by wave numbers $K \gg l^{-1}$, there is no direct interaction between the turbulence and the motion of the large energy-containing eddies. The spectrum in this range of large wave numbers is nearly isotropic, as only the large eddies are aware of the direction of the mean gradient. In this range the spectrum depends only on the parameters that determine the nature of the small-scale flow, so that we can write

$$S = S(K, \varepsilon_{\mathrm{dissV}}, \nu), \quad K \gg l^{-1}. \tag{2}$$

The wave number range $K \gg l^{-1}$ is usually called the equilibrium range. The dissipating wave numbers with $K \approx \eta^{-1}$ and beyond which the spectrum falls off very rapidly, form the high end of the equilibrium range. The lower end of this range, for which $l^{-1} \ll K \ll \eta^{-1}$, is called the inertial subrange, as transfer of energy is only by inertial forces (vortex stretching) in this range. Both production and dissipation are small in the inertial subrange. The production of energy by large eddies results in a peak of $S$ at a certain $K \approx l^{-1}$, and the dissipation of energy causes a sharp drop of $S$ for $K > \eta^{-1}$.

Kolmogorov argued that in the inertial subrange, which is part of the equilibrium range, also $S$ is independent of $\nu$, so that (Kundu and Cohen, 2002):

$$S = S(K, \varepsilon_{\mathrm{dissV}}), \quad l^{-1} \ll K \ll \eta^{-1}. \tag{3}$$

Although little dissipation occurs in the inertial subrange, the spectrum depends on $\varepsilon_{\mathrm{dissV}}$ (viscous dissipation) because the dissipated energy must be transferred across the inertial subrange, from the low to the high wave numbers.

As the units of $S$ is $\mathrm{m}^3/\mathrm{s}^2$ and $\varepsilon$ is $\mathrm{m}^2/\mathrm{s}^3$, dimensional analysis gives (Kundu and Cohen, 2002):

$$S = A\varepsilon_{\mathrm{dissV}}^{2/3} K^{-5/3}, \quad l^{-1} \ll K \ll \eta^{-1}, \tag{4}$$

where $A \approx 1.5$ has been found to be a universal constant, valid for all turbulent flows. Eq. (4) is usually called Kolmogorov's $K^{-5/3}$ law. If the Reynolds number of the flow is large, the dissipating eddies are much smaller than the energy-containing eddies and the inertial subrange is quite broad.

Under the Boussinesq approximation, the energy equation for the instantaneous variables are

$$\frac{\partial \widetilde{T}}{\partial t} + \tilde{u}_j \frac{\partial \widetilde{T}}{\partial x_j} = \kappa \frac{\partial^2 \widetilde{T}}{\partial x_j \partial x_j}. \tag{5}$$

By using Reynolds decomposition, $\tilde{u}_l = U_i + u'$ and $\widetilde{T} = \overline{T} + T'$, the mean heat equation takes the form:

$$\frac{\mathrm{D}\overline{T}}{\mathrm{D}t} + U_j \frac{\partial \overline{T}}{\partial x_j} + \frac{\partial(\overline{u_j T'})}{\partial x_j} = \kappa \frac{\partial^2 \overline{T}}{\partial x_j^2}, \tag{6}$$

where $\kappa$ is the thermal diffusivity.

An equation for the temperature fluctuation intensity $\overline{T'^2}$ can be obtained in a way similar to the one used for obtaining the turbulent kinetic energy. Therefore, the procedure consists of obtaining an equation for $\frac{\mathrm{D}T'}{\mathrm{D}t}$ by subtracting the equation for $\frac{\mathrm{D}T}{\mathrm{D}t}$ and $\frac{\mathrm{D}\overline{T}}{\mathrm{D}t}$ and then multiply the resulting equation for $\frac{\mathrm{D}T'}{\mathrm{D}t}$ by $T'$ and take in the average. The result is

$$\frac{1}{2}\frac{\mathrm{D}\overline{T'^2}}{\mathrm{D}t} = -\overline{wT'}\frac{\mathrm{d}\overline{T}}{\mathrm{d}z} - \frac{\partial}{\partial z}\left(\frac{1}{2}\overline{T'^2 w} - \kappa\frac{\mathrm{d}\overline{T'^2}}{\mathrm{d}z}\right) - \kappa\overline{\left(\frac{\partial T'}{dx_j}\right)}, \tag{7}$$

where $\varepsilon_{\mathrm{dissT}} = \kappa\overline{\left(\frac{\partial T'}{\mathrm{d}x_j}\right)}$ is the dissipation of temperature fluctuation, analogous to the dissipation of turbulent kinetic energy. The first term on the right-hand side of Eq. (7) is the generation of $\overline{T'^2}$ by the mean temperature gradient $\overline{wT'}$, being positive if $\frac{\mathrm{d}\overline{T}}{\mathrm{d}z}$ is negative. The second term on the right-hand side is the turbulent transport of $\overline{T'^2}$.

A wave number spectrum of temperature fluctuations can be defined such that

$$\overline{T'^2} \equiv \int_0^\infty \Gamma(K)\mathrm{d}K. \tag{8}$$

As in the case of the kinetic energy spectrum, an inertial range of wave numbers exists in which neither the production by large-scale eddies nor the dissipation by conductive and viscous effects are important.

As the temperature fluctuations are intimately associated with velocity fluctuations, $\Gamma(K)$ in this range must depend not only on $\varepsilon_{\mathrm{dissT}}$ but also on the variables that determine the velocity spectrum, namely $\varepsilon_{\mathrm{dissV}}$ and $K$. Therefore

$$\Gamma(K) = \Gamma(\varepsilon_{\mathrm{T}}, \varepsilon, K), \quad l^{-1} \ll K \ll \eta^{-1}. \tag{9}$$

The unit $\Gamma$ is $^{\circ}\mathrm{C}^2$ m, and the unit of $\varepsilon_T$ is $^{\circ}\mathrm{C}^2$/s. A dimensional analysis gives

$$\Gamma(K) \propto \varepsilon_{\mathrm{T}} \varepsilon^{-1/3} K^{-5/3}, \quad l^{-1} \ll K \ll \eta^{-1}, \tag{10}$$

which was first derived by Obukhov in 1949 (Kundu and Cohen, 2002). Comparing with Eq. (4), it appear that the spectra of both velocity and temperature fluctuations in the inertial subrange have the same $K^{-5/3}$ form.

## 3. Experimental set up

An infrared camera measures and images the infrared radiation emitted from an object. The fact that radiation is a function of object surface temperature makes it possible, for the camera, to calculate and display this temperature. However, the radiation measured by the camera not only depends on the object temperature but is also a function of the emissivity. Radiation also originates from the surroundings and is reflected in the object. The radiation from the object and the reflected radiation will also be influenced by the absorption of the atmosphere.

Therefore, in order to measure temperature accurately, it is necessary to compensate the effects of a number of different radiation sources. This is done automatically by the camera. The following object parameters must, however, be supplied to the camera:

- The emissivity of the object.
- The reflected temperature.
- The distance between the object and the camera.
- The relative humidity.

To find the emissivity of the smoke in the near wake, we select a reference point and measure its temperature using a thermocouple. Then, we alter the emissivity until the temperature measured by the camera agrees with the thermocouple reading. This is the smoke emissivity value we use in our work ($\varepsilon = 0.1$). It is also required that the temperature range be far from the ambient temperature, a condition met in the present work.

The measurement distance is set to one meter to reduce the radiation absorbed by the atmosphere.

### 3.1. Measurement formula

The camera receives radiation from both the object itself and from the surroundings via reflection over the object's surface. Both radiation contributions are attenuated to some extent by the atmosphere in the measurement path. To these two contributions we must add a third radiation contribution from the atmosphere itself.

We can use Fig. 1 to derive a formula for the calculation of the object temperature from the calibrated camera output.

Assuming that the received radiation power $W$ from a blackbody source at temperature $T_{\mathrm{source}}$ over a short distance generates a camera output signal $U_{\mathrm{source}}$ and is proportional to the power input (power linear camera), we can write

$$U_{\mathrm{source}} = C(W_{\mathrm{source}}), \tag{11}$$

$C$ is a constant given by one of the expressions below according to the kind of source considered.

When the source is a gray-body with emissivity $\varepsilon$, the received radiation is $\varepsilon W_{\mathrm{source}}$.

The three collected radiation power terms are:

1. Object emission $= \varepsilon\tau W_{\mathrm{obj}}$, where $\varepsilon$ is the emissivity of the object and $\tau$ is the transmittance of the atmosphere. The object temperature is $T_{\mathrm{obj}}$.

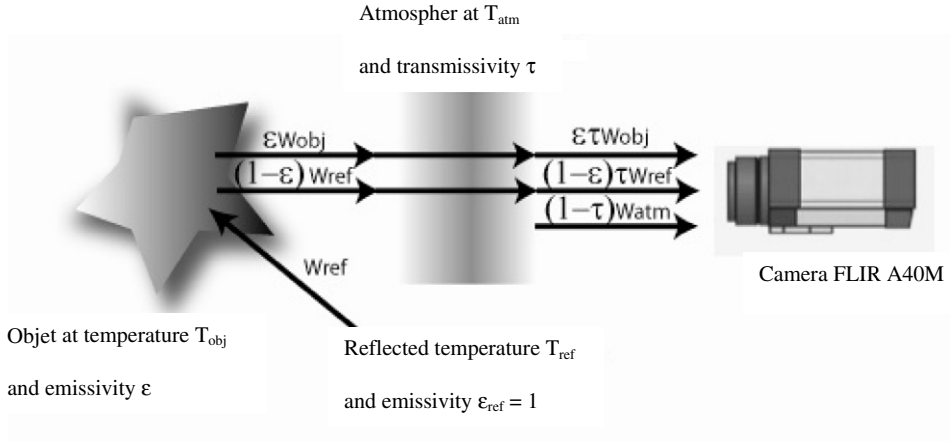


Fig. 1. A schematic representation of the general thermographic measurement situation.

2. Reflected emission from ambient sources $= (1-\varepsilon)\tau W_{\text{refl}}$, where $(1-\varepsilon)$ is the reflectance of the object. The ambient sources have the temperature $T_{\text{refl}}$.
3. Emission from the atmosphere $= (1-\tau)W_{\text{atm}}$, where $(1-\tau)$ is the emissivity of the atmosphere. The temperature of the atmosphere is $T_{\text{atm}}$.

The total received radiation power can now be written:

$$W_{\text{tot}} = \varepsilon\tau W_{\text{obj}} + (1-\varepsilon)\tau W_{\text{ref}} + (1-\tau)W_{\text{atm}}. \quad (12)$$

This can be transformed to obtain the output signal of the camera:

$$U_{\text{tot}} = \varepsilon\tau U_{\text{obj}} + (1-\varepsilon)\tau U_{\text{ref}} + (1-\tau)U_{\text{atm}}. \quad (13)$$

Solving for $U_{\text{obj}}$, we obtain:

$$U_{\text{obj}} = \frac{1}{\varepsilon\tau}U_{\text{tot}} - \frac{1-\varepsilon}{\varepsilon}U_{\text{ref}} - \frac{1-\tau}{\varepsilon\tau}U_{\text{atm}}. \quad (14)$$

This is the general measurement formula used in all FLIR Systems thermographic equipments.

The camera is calibrated by FLIR systems (Table 1). The camera measures a luminance taking into account of all the parameters. This quantity is known as "non-compensated". The operator introduces the object parameters. It allows the compensation determination. From this, one gets the object luminance (compensated) from an equivalent black body.

It is enough to defer this compensated value on the calibration curve to obtain the real temperature.

Thus, the measurement is done according to the following procedure. First of all the following assumptions are made:

- The smoke is opaque.
- The emissivity is gray and denoted $\varepsilon_0$.
- The surface temperature is $T_{\text{obj}}$.
- The environment is comparable to a black body of temperature $T_{\text{env}}$.
- The atmosphere is comparable to a black body of temperature $T_{\text{atm}}$.
- The atmosphere transmission is imperfect and worth $\tau_{\text{atm}}$.

According to relation (3), the luminance ($L'$) as seen by the camera is equal to

$$L' = \tau_{\text{atm}}\varepsilon_0 L_{\text{obj}} + \tau_{\text{atm}}(1-\varepsilon_0)L_{\text{env}} + (1-\tau_{\text{atm}})L_{\text{atm}}. \quad (15)$$

Considering that $T_{\text{env}} = T_{\text{atm}}$ and that transmission is optimum, this relation simplifies to

$$L' = \varepsilon_0 L_{\text{obj}} + (1-\varepsilon_0)L_{\text{env}}. \quad (16)$$

The temperature is then obtained from the calibration curve (Fig. 2).

### 3.2. Camera characteristics

We use a matrix camera of 320 × 240 pixels. One needs at least 3 detectors to have a correct measurement. The smallest object the camera will be able to measure is equal to shot $\times \frac{3}{320}$. Knowing the distance between the object and the camera, the width of the shot being given by Fig. 3 is

$$\text{Shot width} = 2 \times D \times \tan\frac{\alpha}{2}. \quad (17)$$

The objective of the camera being of 24°, the smallest object the camera can detect is $3.89 \times 5.19\ \text{mm}^2$ (Table 2). The temperature measured is then averaged over a surface of $3.89 \times 5.19\ \text{mm}^2$.

### 3.3. The cylinder deformation device

The radially deforming cylinder is made out of PVC. The cylinder deformation are obtained using a circular cam (Fig. 4) whose radius is varied according to the following sinusoidal law:

$$a = a_0[1 + (\Delta a/a_0)\sin(2\pi F_d t)]. \quad (18)$$

Table 1
Main features of the IR camera FLIR A40M

| Characteristic | Value or description |
|---|---|
| Object temperature measurement range | −40/ + 120 °C<br>0/+500 °C<br>+500/1700 °C |
| Measurement accuracy | ±2 °C or ±2% of the recording. The specification is valid when the ambient temperature lies between +5 °C and +45 °C |
| Thermal sensitivity | 80 mK at 25°C |
| Detector type | Matrix in focal plan (FPA), microbolometer not cooled |
| Spectral range | 7.5–13 μm |
| Integration time | 20 ms |
| Distance range between camera and object | >0.3 m |
| Spatial resolution | 320 × 240 pixels |

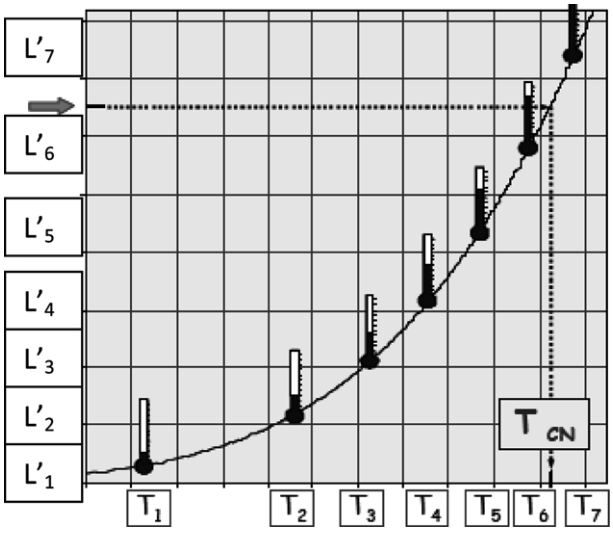


Fig. 2. Calibration curve.

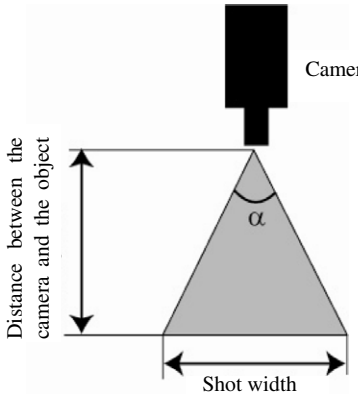


Fig. 3. Relation between the distance camera–object and the shot width.

Table 2
Estimation of object minimal size

| Distance between the camera and the object | Shot width | Minimal size of the object allowing to have an accurate response (mm) |
|---|---|---|
| 500 mm | 212 mm | 1.99 × 2.65 |
| 1 m | 415 mm | 3.89 × 5.19 |
| 5 m | 2.075 m | 19.45 × 25.94 |

The rotation of the cylinder axes is ensured by an electric motor. The cam geometry makes it possible to have for each engine turn four radial cylinder deformation cycles. Then, we have

$$F_d = 4N/60. \tag{19}$$

Balls were inserted in uniformly distributed cavities on the ring outer surface of diameter equal to the minimal diameter of the deformable cylinder. The unit movement can be divided into two phases. First, the cams push the balls. The balls push the deformable cylinder interior wall outward. The second phase is that of the return of the balls to their initial positions. The cylinder wall returns to its initial state. This dynamics allows the increase and the reduction diameter according the sinusoidal law presented previously (18).

### 3.4. Setup experiments and measurements procedure

The tests are carried out in a low intensity turbulence DELTALAB subsonic wind tunnel of section 450 × 300 mm$^2$, usually used for "hot wire" sensor calibration.

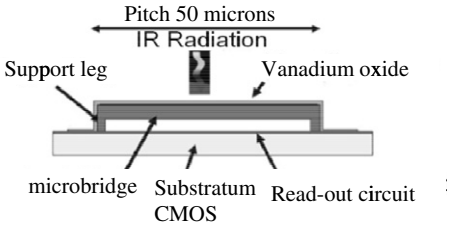


Fig. 5. Diagram of a detector.

A smoke generator and an infra-red camera are used for flow visualization.

Temperature and flow structure variations are recorded using a Thermovision FLIR A40M camera. The camera speed is 60 images per second. The work area and the vision field are determined by the objective being used(Table 2). The thermal detector (Bolometer) is a thermistance which becomes overheated according to the absorbed flow (Fig. 5). The control of the temperature of the micro bolometer is essential.

#### 3.4.1. Studied parameters definition

The objective of this work is to investigate the near wake flow structure generated by a radially deforming cylinder via infrared thermography. We examine the flow temperature mean field and temperature fluctuating field along the wake center line. Temperature fluctuations are measured using an infra-red camera for a Reynolds number $Re = 1700$ and a deformation of 5% of the initial diameter.

The Reynolds number is given by

$$Re = 2U_\infty a/v, \tag{20}$$

where $U_\infty$ is the velocity far upwind from the cylinder (0.64 m/s in this work), a is the cylinder radius (0.02 m) and $v$ is the air kinematic viscosity. According to Kovasznay (1970) when the aspect ratio is equal to or higher than 4, edge effects are of a tiny influence on the flow central part and can thus be neglected. We fixed our aspect ratio to 6.

Temperature and the distance are made non-dimensional by using the average temperature on the wake center line $T_{moy}$ and the cylinder diameter $d$ respectively. The reference origin is the cylinder center. $x$ and $y$ are the flow direction and the transverse direction respectively (Fig. 6).

The measurements are taken over a length $x = 6 * d$ along the wake center line. The evaluation of the average

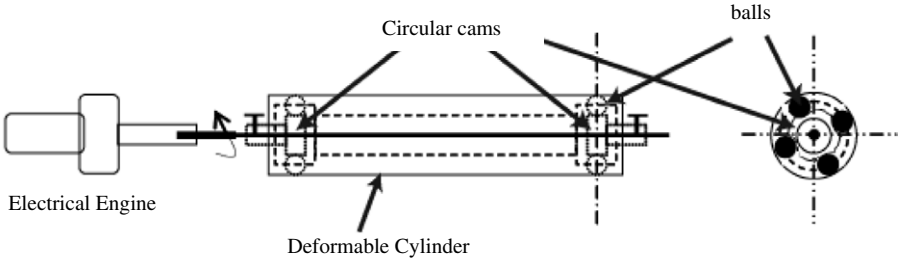


Fig. 4. Mechanism for cylinder deformation.

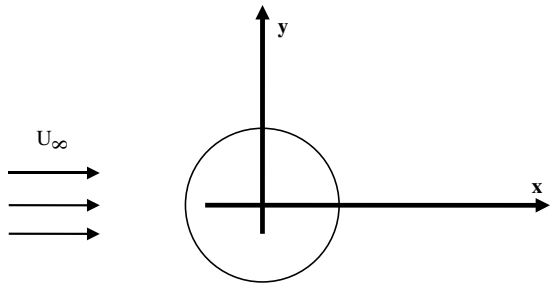


Fig. 6. Coordinates system.

temperature and the fluctuation root mean square (r.m.s.) are calculated using the following relations:

- Temperature mean field

$$T = T_{\text{moy}} + T'_{\text{m}}, \tag{21}$$

where $T$ is the mean temperature at a point on the wake center line for one shedding period (temporal average). $T_{\text{moy}}$ is the mean temperature on the wake center line (space average) and $T'_{\text{m}}$ is the temperature fluctuation.

- The mean temperature on a part of the wake center line is calculated using the following relation:

$$T_{\text{moy}} = \frac{\sum_{i=1}^{i_{\max}} T_i}{i_{\max}}, \tag{22}$$

where $i$ is the number of temperature measurement points $T$ which are taken on the wake center line.

- The root mean square (rms) is calculated as follows:

$$\text{rms} = \sqrt{(T'_m)_i^2}. \tag{23}$$

### 3.4.2. Measurement procedure

The cylinder is placed perpendicularly to the fluid flow. Its axis is horizontal. The infra-red camera is fixed on a tripod so that the image is perpendicularly focused on the cylinder and its vicinity (principally on the downstream area because it constitutes the wake development area).

We inject hot fluid from a smoke generator. This fluid is convected by eddies developed behind the cylinder. A thermocouple is placed in the fluid flow (in the smoke flow). This point is visible on the camera screen. According to the value displayed by the thermocouple, one fixes the camera required data to carry out an exact measurement of the temperature.

Once the test parameters are regulated (flow rate, smoke flow, ..., etc), the infra-red camera is actuated to record the flow. The first test is carried out on a non-deformable cylinder. Then, we vary the electric motor rotational speed to have the various deformation frequencies. The recording lasts 60 s.

## 4. Results

### 4.1. Non-deformable cylinder

A study of a non-deformable cylinder wake is necessary to have a basis for comparison. Smoke is hotter than the fluid flow. The vortices formed behind the cylinder transport those temperature variations along the wake. At a point on the wake center line, located on the carrying energy vortex way, we measure the temperature. This point will see its temperature vary at the rhythm of the elapsing vortices. Temperature increases as they pass and decreases thereafter.

#### 4.1.1. Vortices shedding frequency

Fig. 7 shows the temperature variation signal taken at the point ($x/d = 4$) on the wake center line. The signal spectral analysis (Fig. 8) shows the existence of many frequencies. The largest spectrum peak corresponds to the natural vortex shedding frequency. The other peaks correspond to smaller vortices carrying weaker thermal energy. As the selected point is on the wake center line, the temperature at this point is influenced by both sides' emitted vortices (upper and lower faces). The detected frequency is twice the shedding frequency. In the present study, the vortices natural shedding frequency is $F_0 = 3.30$ Hz. The non-dimensional number characterizing the vortex shedding is the Strouhal number. This number is given by the following relation:

$$St = 2F_0 a/U_\infty. \tag{24}$$

In this study, the natural Strouhal is $St = 0.21$.

#### 4.1.2. Characteristics of the near wake

In Fig. 9, we note that the wake is divided into three main zones. Zone 1 is imprisoned between the cylinder

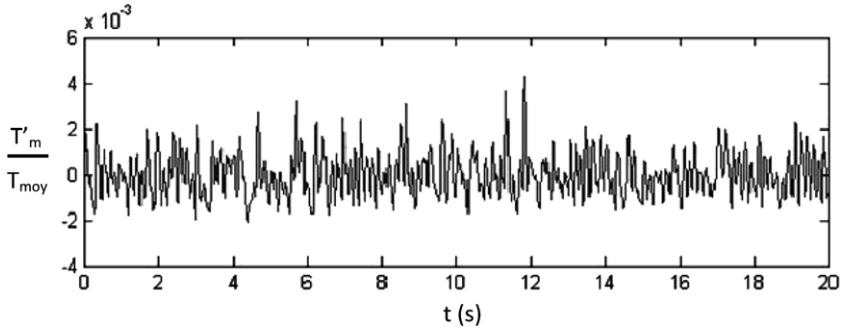


Fig. 7. Mean temperature signal at a point located at $x/d = 4$, on the wake center line for the non-deformable cylinder.

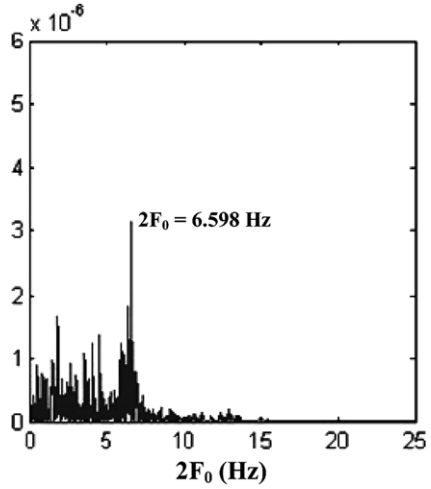


Fig. 8. Spectrum of temperature fluctuations at a point located at $x/d = 4$, on the wake center line for a non-deformable cylinder.

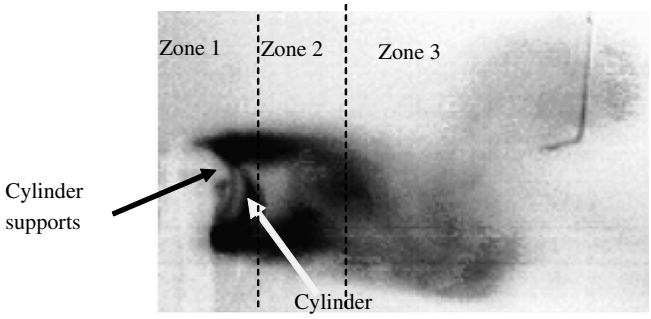


Fig. 9. Position of the wake zones.

downstream wall and the vortices in formation. It is characterized by a low smoke density (low temperatures on the curves) compared to the second zone which has the most important smoke density in the near wake. The distribution of the mean thermal field (Fig. 10) shows that Zone 1 is colder than the Zone 2, because the smoke thermal energy transported by the vortices does not penetrate this area. Therefore, the flow in Zones 1 and 2 are of different nature.

Konstantinidis et al. (2003), noticed the formation of a recirculation bubble between the downstream cylinder wall and the vortex formation area for several Reynolds numbers, namely $Re = 1550$, $Re = 2150$, $Re = 2750$, and $Re = 7450$. They explained it by the appearance of a flow in the opposite direction of the main flow (negative speed in the direction of the main flow). The length of this bubble is given starting from the center of the cylinder up to the point on the near wake center line where the speed in the flow direction is zero.

In Fig. 10, we note that Zones 1 and 2, are spread out over a length of $2^{*} d$ over the center line, starting from the center of the cylinder. To characterize these two zones, we draw the distribution of the mean temperature over a length of $2^{*} d$ on the wake center line (Fig. 11). We propose to consider that this dead fluid area is initiated on the cylinder downstream wall and ends where the vortex formation area starts. Therefore, the length $L_b$ of this area is defined as follows: It is the distance between the cylinder center and the first point where the temperature fluctuation cut the $x$-axis for the first time ($T'_m = 0$) (Fig. 12). Therefore, $L_b = 0.82^{*} d$. We consider this definition owing to the fact that the temperature is considered as a passive tracer. The required point is a point where the axial velocity is zero. So, the hot smoke stagnates in this point and is not evacuated by the vortices. The temperature is then constant and its fluctuations are null.

While moving away towards the downstream recirculation zone, smoke becomes increasingly dense. It is the start of Zone 2 (vortices formation zone). In the vortex center the smoke density is maximal. The mean temperature fluctuation takes its max positive values. This area is characterized by a characteristic length which is the length of vortex formation, $L_f$. To determine this length, we draw the rms distribution of the temperature fluctuations normalized by the mean temperature along the wake center line (Fig. 13).

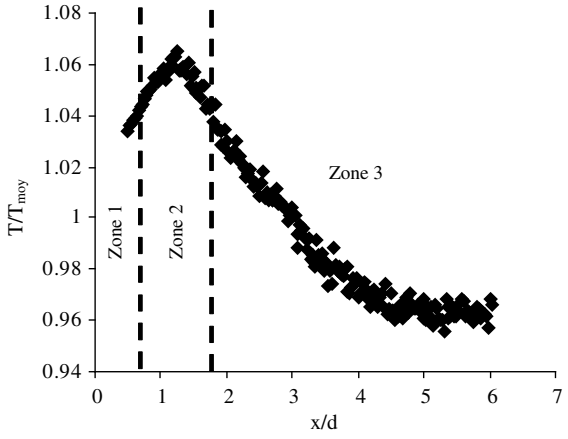


Fig. 10. Temperature distribution along the wake center line.

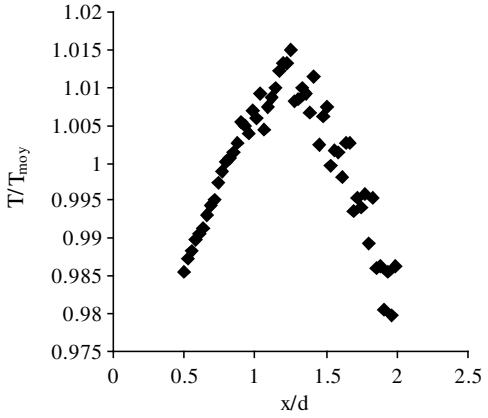


Fig. 11. Mean temperature distribution along the wake center line (zoom of Fig. 10).

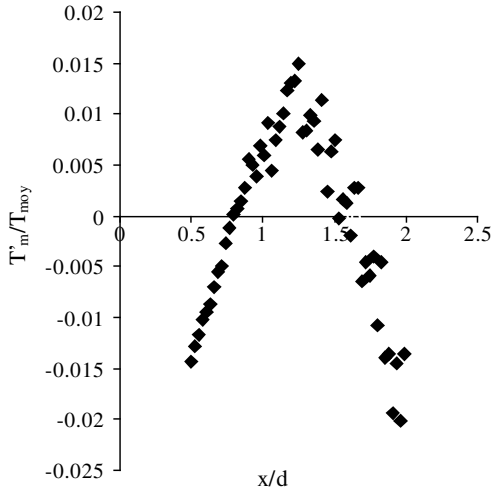


Fig. 12. Temperature fluctuation distribution along the wake center line.

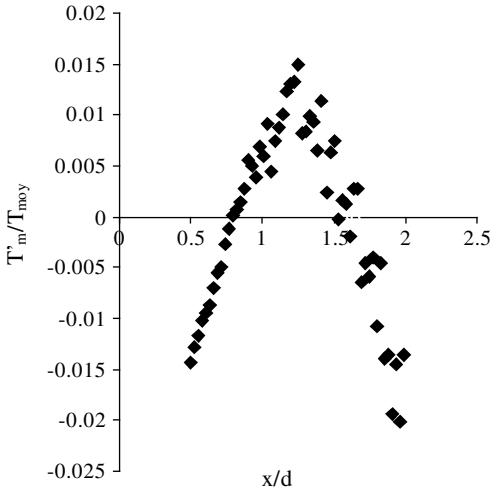


Fig. 13. rms distribution of the temperature fluctuations along the wake center line.

In Fig. 13, the rms distribution of the temperature fluctuations shows that the turbulence rate (the fluctuations intensity) is highest in the vortex formation zone. It is characterized by a peak from which the length of vortex formation is given by analogy with the maximum of the velocity rms (Griffin, 1995). We find $L_f = 1.25^{*} d$.

Another characteristic length can be inferred from the curve in Fig. 11. It is the vortex characteristic radius, $R_t$. In the formation zone, the first vortex boundary starts beginning from the point where the temperature $T$ is equal to the temperature $T_{moy}$ ($T = T_{moy}$). Then, it increases until it reaches a maximum temperature (top of the peak). The curve (Fig. 13) shows that this peak is characterized by maximum turbulence intensity (vortex center). So, we define the vortex characteristic radius as follow: it is the distance along the $x$-axis between the point where the temperature fluctuations are zero (Fig. 12) and the point where we the peak of the fluctuations (vortex center) is reached. Therefore, $R_t = 0.43^{*} d$.

### 4.2. Deformable cylinder

#### 4.2.1. Vortex shedding frequency

In this section, we examine the radial deformation effect on the vortex shedding frequency. For several deformation frequencies, we draw the temperature variation at the considered point for the non-deformable case (Fig. 14). We note, on Fig. 14, that the mean temperature increases until it reaches a maximum around $F_d/F_0 = 2$. Then, it decreases, thereafter, when this ratio is increased.

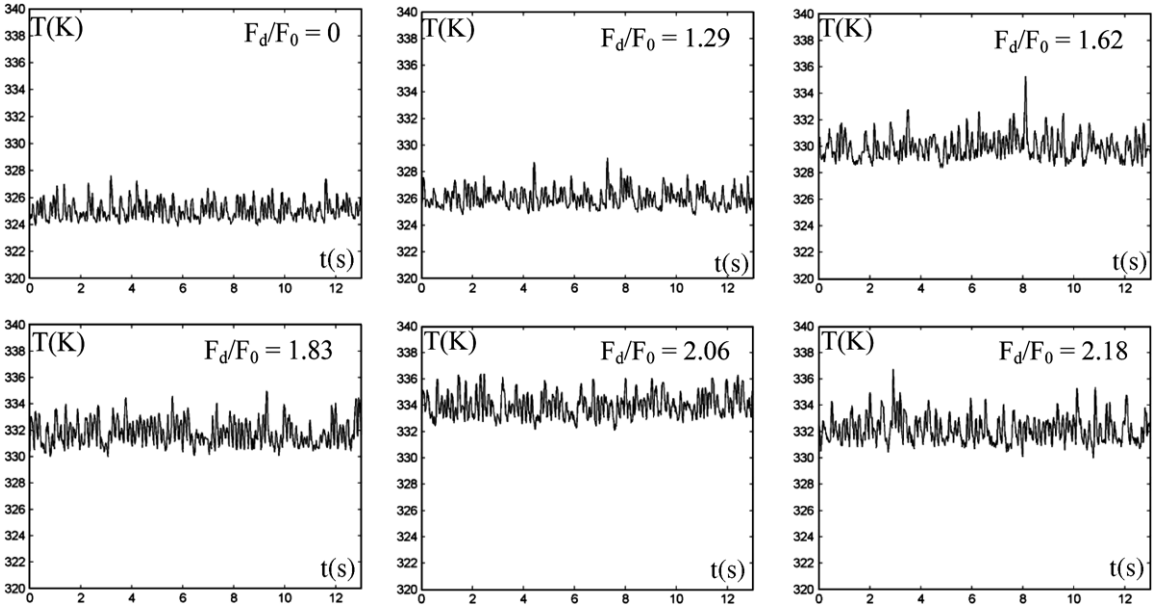


Fig. 14. Temperature fluctuations at $x/d = 4^{*} d$ along the wake center line for different deformation frequencies.

Fig. 15, shows the mean temperature fluctuation spectra. We consider a deformation frequency range normalized by the natural shedding frequency between $F_d/F_0 = 1.29$ and $F_d/F_0 = 3.66$.

It is to be noted that there is a vortex shedding frequency amplitude modulation by the imposed deformation frequency. The spectra present a broad band of peaks around the natural shedding frequency and additional peaks characterizing smaller wake vortices.

Following this amplitude peak evolution in the considered deformation frequency range, one clearly note that the energy level of the peaks is most important for the two frequency ratios $F_d/F_0 = 1.92$ and $F_d/F_0 = 2.04$. This indicates that there is a "Lock-in" frequency range between these two ratios.

The experiments of Tanida et al. (1973) show that the "Lock-in" range for an oscillating cylinder is closed to twice the vortex natural shedding frequency. The same experimental result was found by Konstantinidis et al. (2003) for a static cylinder and a periodically disturbed flow. Fundamental "Lock-in" is obtained for disturbance frequencies around twice the vortex shedding frequency.

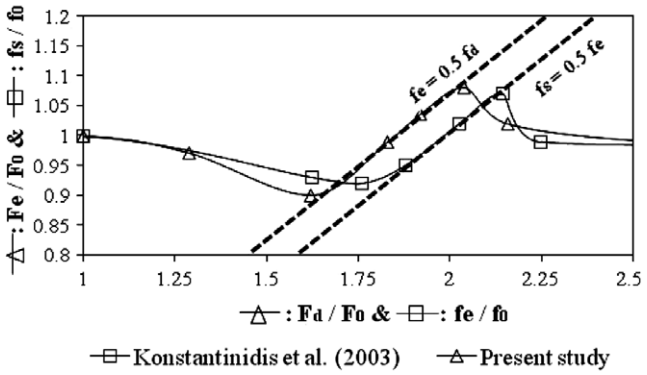


Fig. 16. Shedding frequency variation versus the deformation frequency $F_d/F_0$ (present study) and versus the periodically disturbed flow frequency $f_s/f_0$ (Konstantinidis et al., 2003).

By analogy, we note, in Fig. 15, that there is a transition from the modulation towards the synchronization of the two frequencies (capture of the shedding frequency by the deformation frequency) for deformation frequencies close to twice the natural shedding frequency, between $F_d/F_0 = 1.92$ and $F_d/F_0 = 2.04$.

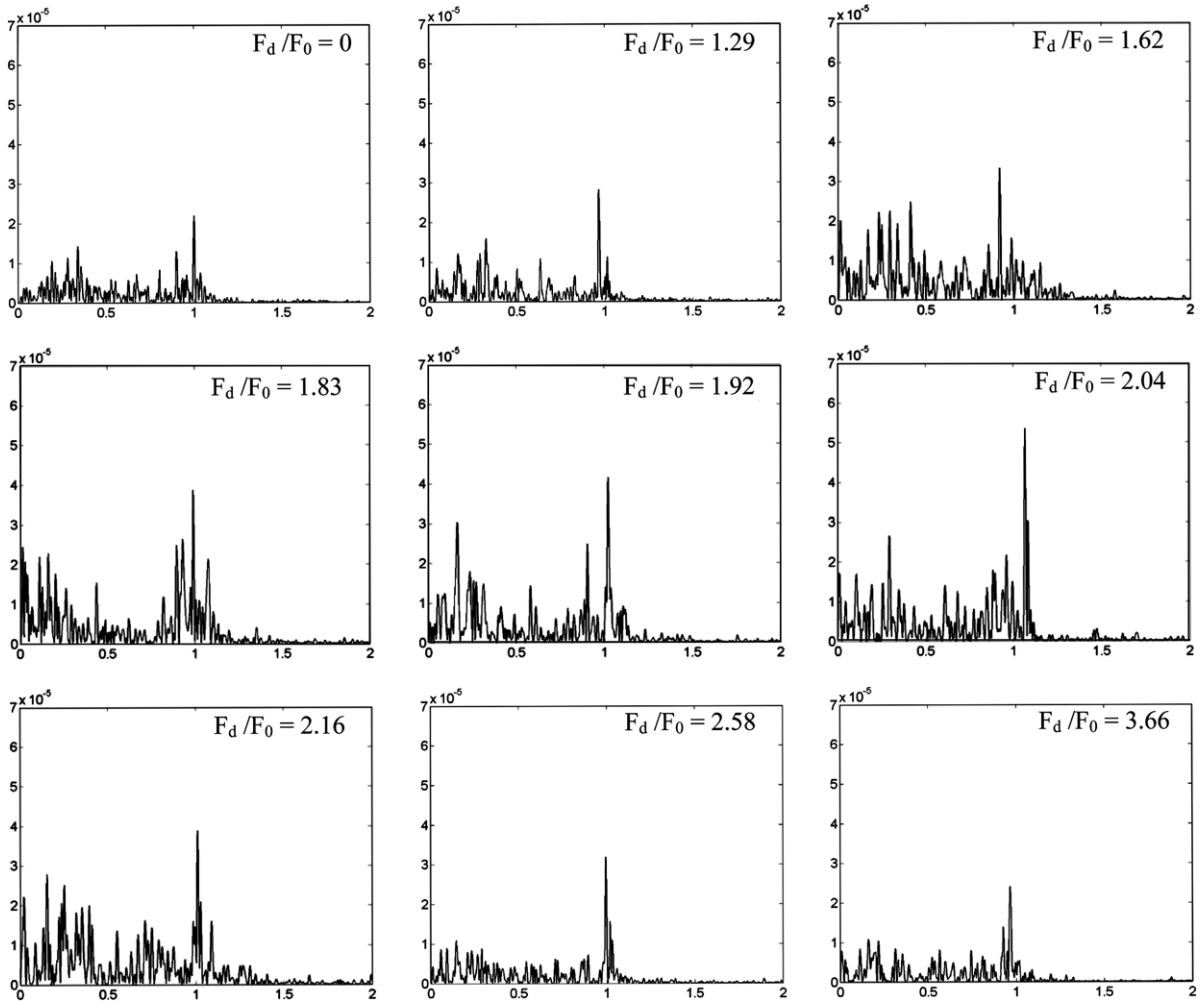


Fig. 15. Spectra of the temperature fluctuations at $x/d = 4$ along the cylinder center line for various deformation frequencies.

The synchronized wake frequency is obtained when the deformation frequency is twice the natural shedding frequency. The spectra show peaks with a narrow band, well established at this frequency. Thus the "Lock-in" is obtained. The periodic amplitude of the wake temperature fluctuations related to the vortex shedding is undeniably more important in the vicinity of the "Lock-in" range.

Fig. 16 shows the shedding vortex frequency variations according to the cylinder deformation frequency. The values are normalized by the natural shedding frequency. The values of the vortex shedding frequencies correspond to the positions of the maximum peaks on the signal spectra (Fig. 15), representing the variation in the mean temperature at a point on the wake center line. Comparing this curve with Konstantinidis et al. (2003) (Fig. 16), it is noted that the vortex shedding frequency varies in a way similar to the one for a radial cylinder deformation, or for a periodic disturbance imposed to the velocity of the incoming flow. We note that for deformation frequencies close to the fundamental range of "Lock-in", the two curves give practically the same vortex shedding frequencies (Fig. 16). Indeed, we note that we obtain the same slope but, in the case of the radial deformation, the "Lock-in" is started slightly advanced.

### 4.2.2. Near wake characteristics

We will now study the effect of the cylinder radial deformation on both the wake center line temperature mean

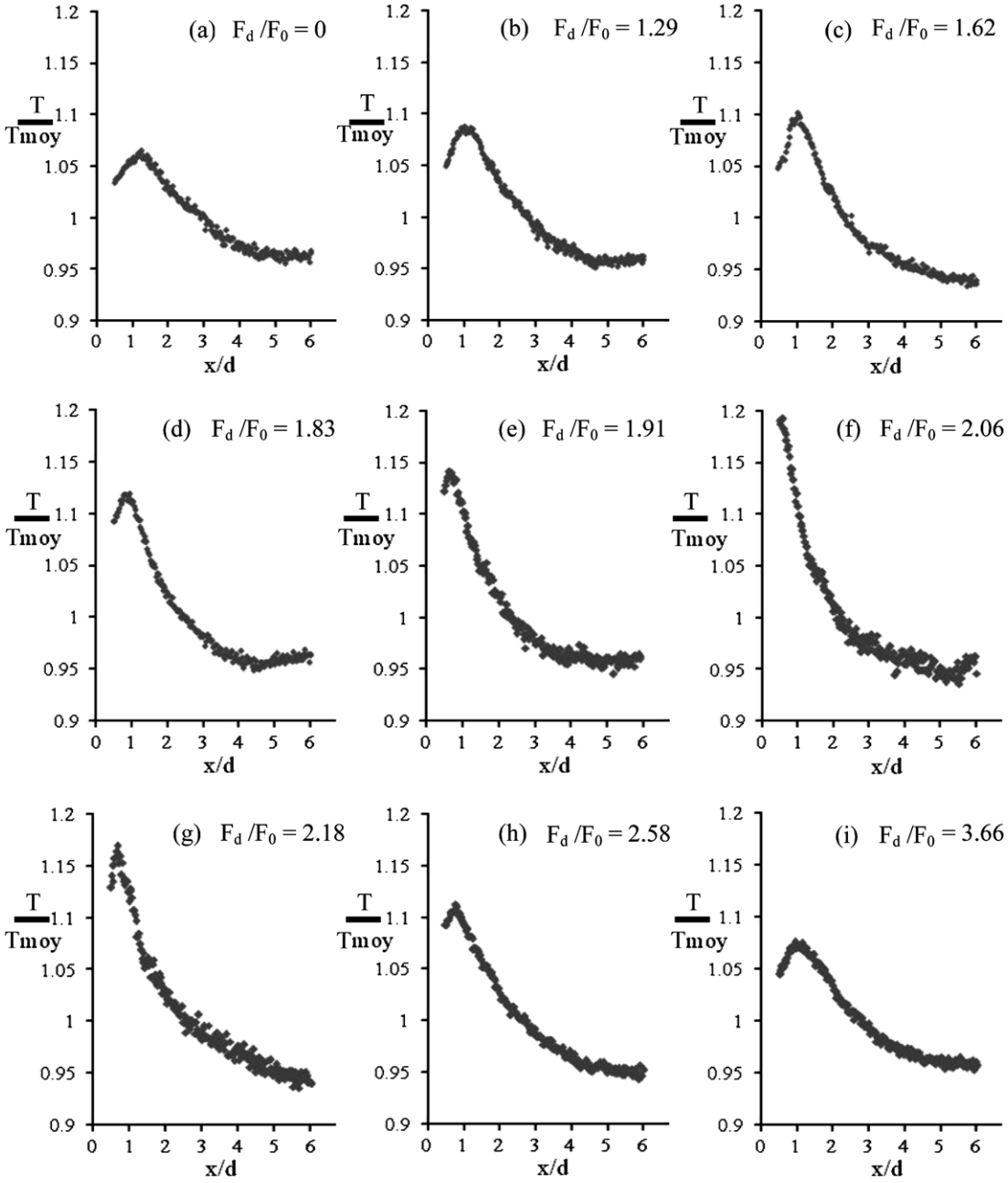


Fig. 17. Mean temperature distribution along the wake center line.

field and fluctuating field distributions. Fig. 17a–i shows that the general look of the mean temperature field distribution is the same as the one we had for the non-deformable case.

In the vicinity of the cylinder downstream wall (recirculation zone), the mean temperature increases gradually until it reaches the point characterizing the beginning of the vortices formation zone. Then, it increases abruptly towards its maximum value, characterized by a peak, from which the formation length is measured. Then, it decreases towards temperatures equal to those at the beginning. Then, it is spreads out, asymptotically along the remote wake. However, one notices, in the curve (Fig. 17a–i), that the formation zone is moved slightly towards the cylinder, showing a light penetration of the recirculation zone by the vortices during their formation.

In Fig. 17b–d, we note that the initial increase in the temperature is reduced when one increases the frequency of deformation. This zone disappears completely in the vicinity of the "Lock-in" frequency (Fig. 17e and f). This indicates that the vortices penetrate the recirculation zone completely and that they develop directly on the downstream cylinder wall. The formation zone continues to approach the cylinder and its maximum temperature (the peak of the temperature) increases proportionally according to the deformation frequency. On the other hand, the dimension of this zone is inversely proportional to the deformation frequency.

Increasing the deformation frequency further (Fig. 19g–i), one notices that the phenomena observed for the two preceding deformation frequencies are completely reversed. The curve starts to take again the same look as the one of the non-deformable case. It loses its monotony as the frequency of deformation increases. The recirculation zone is then initiated in the vicinity of the cylinder and the formation zone moves more and more away from the cylinder. Its maximum temperature (top of the peak) decreases and its dimension increases compared to the preceding two cases (Fig. 19e and f).

Fig. 18 shows the distribution of the fluctuating temperature field along the wake center line. It is noted that it is maximum in the vortices formation zone for all the deformation frequencies. But, it varies from one frequency to another. The temperature fluctuations in the vortices for-

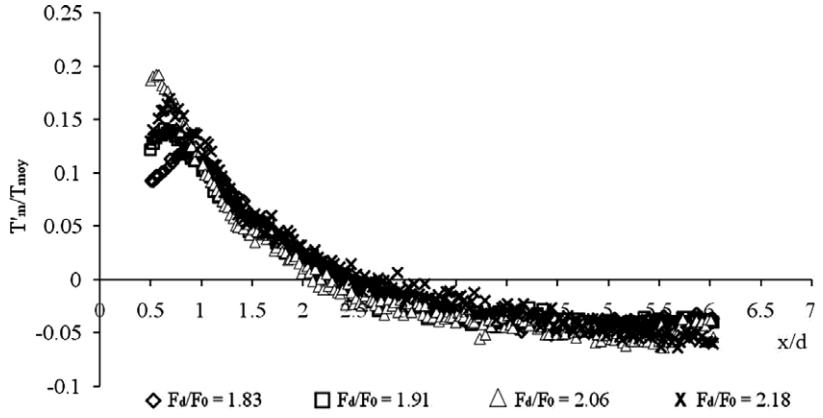


Fig. 18. Non-dimensional temperature fluctuation distributions along the wake center line.

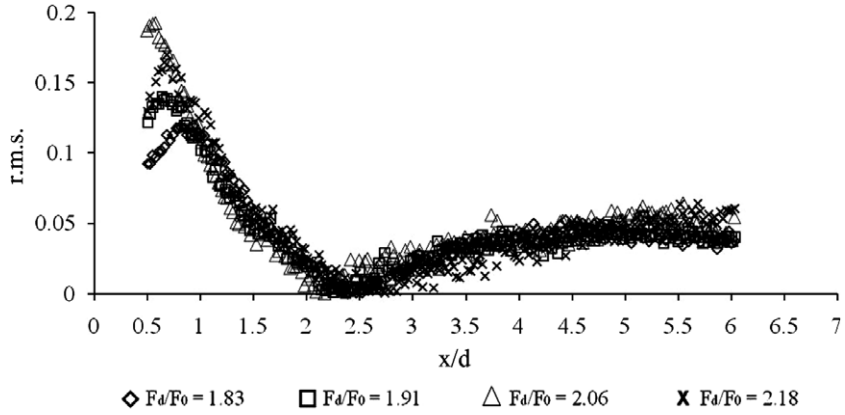


Fig. 19. Distribution of the r.m.s.

mation zone are more important for the deformation frequencies close to the fundamental range of "Lock-in" ($F_d/F_0 = 1.92$ and $F_d/F_0 = 2.04$).

The temperature rms on the wake center line (Fig. 19) also presents a turbulence maxima in the vortex formation zone. The rate of turbulence, in this zone, varies according to the deformation frequency. It is noted that it increases when the deformation frequency increases, reaches a maximum value in the vicinity of the "Lock-in" frequency, and decreases when we continue to increase the deformation frequency higher than the "Lock-in" frequency.

To better characterize the two zones (recirculation zone and formation zone), we draw the mean temperature fluctuation distribution over a length of ($2 * d$) along the wake center line for the previous deformation frequencies (Fig. 20).

It is noted that for the frequency ratios $F_d/F_0 = 1.29$, $F_d/F_0 = 1.62$ and $F_d/F_0 = 1.83$, the length of the recirculation zone decreases slightly as compared to the non-deformable case. Then, it disappears completely when the deformation frequency is close to the fundamental range of the "Lock-in" ($F_d/F_0 = 1.91$ and $F_ds/F_0 = 2.06$). While moving away from this range, the recirculation zone reappears and takes again its natural dimensions.

According to the preceding results, we draw the evolution of the various characteristics of the near wake according to the deformation frequency.

In the vortex formation zone, the rate of turbulence is more important when compared to the other wake zones. This zone is characterized by a peak, indicating the maximum of the temperature fluctuation rms on the wake center line.

The variation of length of formation zone according to the deformation frequency was drawn following the positions of the peak positions for each deformation frequency. Fig. 21 shows that the formation length is minimal when

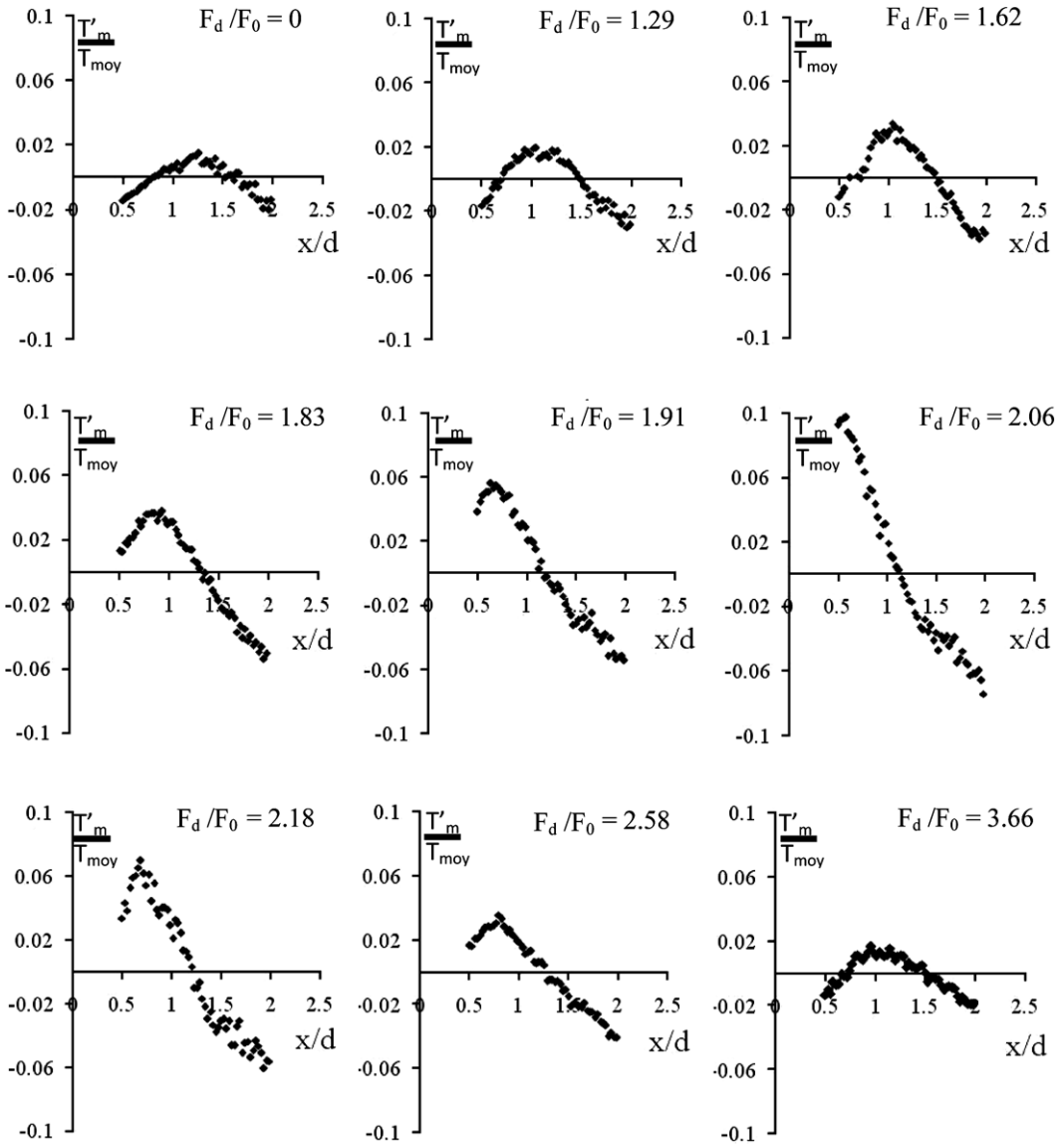


Fig. 20. Distribution of the temperature fluctuation along the wake center line.

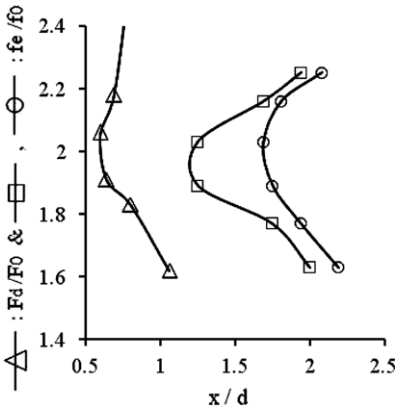


Fig. 21. —△—: Position of the maximum temperature fluctuation along the wake center line (present study). —□— $(u'/U)_{max}$; —○— $(v'/U)_{max}$: Position of the maximum velocity fluctuation along the wake center line (Konstantinidis et al. (2003)).

the deformation frequency is close to the fundamental range of "Lock-in". Comparing the curve of this study with that given by Konstantinidis et al. (2003) (Fig. 21) where $f_e$ is the flow disturbance frequency, it is noted that they have the same look as for a uniform flow around a radially deformable cylinder or for a periodically disturbed flow (periodic velocity) around a static cylinder. The study of the thermal field led to the same results as those of the velocity field. The only noticeable difference is that the radial deformation destroys Zone 1 when the deformation frequency is close to the "Lock-in" frequency, i.e. twice the natural shedding frequency. So the vortex center in the formation zone is much closer to the downstream wall of the cylinder than in the case considered by Konstantinidis et al. (2003) (Fig. 21).

For each deformation frequency, there is a maximum value of the temperature fluctuations rms corresponding to the peak position coordinates of the formation zone (Fig. 19). Fig. 22 clearly shows that the turbulence rate is relatively weak for a deformation frequency far from the

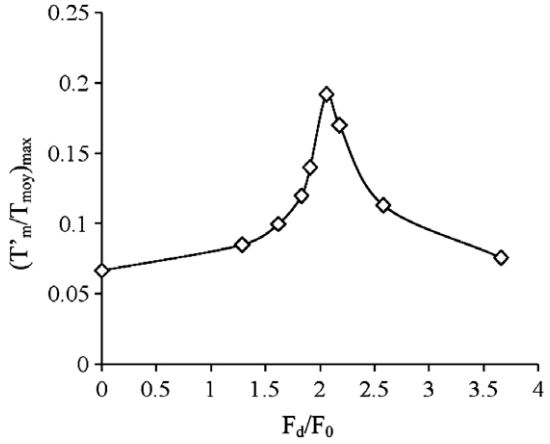


Fig. 22. Plot of maximum of the temperature fluctuations peaks versus the frequency deformation.

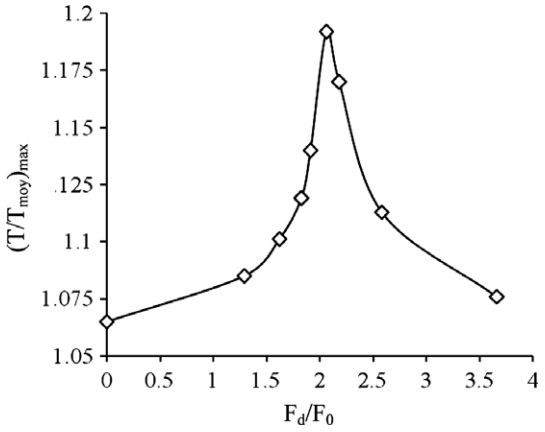


Fig. 23. Temperature maximum versus the deformation frequency.

"Lock-in" fundamental range and is important in this range.

The maximum wake mean temperature is recorded at the vortex center and corresponds to the formation zone peak position. The mean temperature at this point varies according to the deformation frequency (Fig. 23). Mean temperature and turbulence rate exhibit the same variation trend. Also notice that the thermal energy transported by the vortices is more important for deformation frequencies close to the fundamental range of "Lock-in". Hence, for the deformable cylinder close to the "Lock-in" frequency, there is much more energy transported by the wake vortices than for the non-deformable cylinder. The wake is hotter for deformable cylinder than for the non-deformable cylinder.

Having seen the cylinder deformation influence on both the turbulence rate and the maximum temperature in the formation zone, we look now at the modification of the size of the vortices developed in the formation zone.

With monitor the vortex dimensions over one period. Previously, we defined (for the non-deformable cylinder case) a characteristic length, $R_t$, indicating the vortex characteristic radius. Fig. 24, shows that the vortex size is sensitive to the cylinder deformation frequency. For a deformation frequency close to the fundamental range of

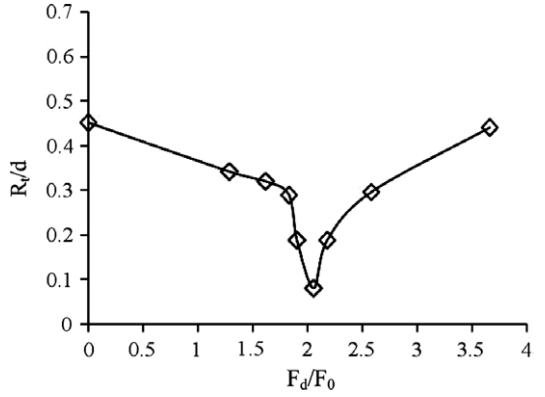


Fig. 24. Characteristic radius function of the frequency deformation.

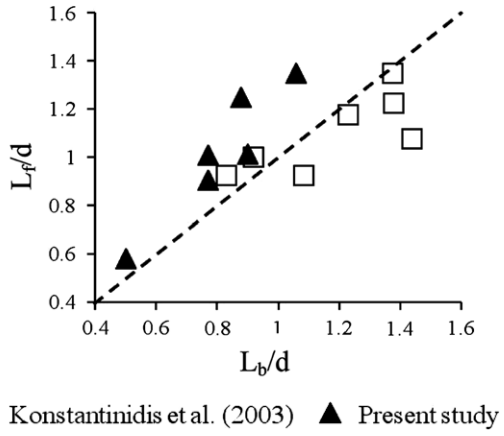


Fig. 25. Relation between the dimensions of the recirculation zone and the formation zone.

"Lock-in", the vortex characteristic radius is minimal. Out of this range, the characteristic radius increases gradually until it reaches its initial length (its length in the non-deformable cylinder case).

The recirculation zone length is related to the way the vortices develop and to the vortex position. It was seen previously that the formation zone length and the characteristic radius of the vortex vary according to the deformation frequency. These variations cause modifications of the recirculation zone length. Fig. 25 shows a plot of the formation zone length versus the recirculation zone length. There is a linear relationship between these two characteristic lengths. The noise in the data are due to experimental errors. The present results agree well with those of Konstantinidis et al. (2003) (Fig. 25).

## 5. Conclusion

The present experimental study was aimed at examining the cylinder radial deformation influence on the near wake characteristics. An infrared experimental technique was employed to reach this objective. Hot smoke was injected within the flow using a smoke generator. We used a thermovision FLIR A40M camera to record the evolution of the temperature variations, which were advected by the developed vortices in the deformable cylinder wake. The camera allowed detailed flow observations.

This study was carried out for a Reynolds number, $Re = 1700$. We studied the non-deformable case and eight deformation frequencies, namely: $F_1 = 4.27$ Hz, $F_2 = 5.34$ Hz, $F_3 = 6.04$ Hz, $F_4 = 6.34$ Hz, $F_5 = 6.73$, $F_6 = 7.13$ Hz, $F_7 = 8.51$ Hz and $F_8 = 12.08$ and. The "Lock-in" phenomenon corresponds to the vortex shedding frequency being captured by the cylinder radial deformation frequency. This phenomenon occurs as for the periodically disturbed flow (periodic disturbances imposed to flow velocity) around a static cylinder, and in the case of a uniform flow around an oscillating cylinder. The "Lock-in" for radially deformable cylinder occurs for a frequency close to twice the natural shedding frequency (Von-Karman street).

The vortex formation length and the recirculation bubble length vary with the deformation frequency and they are reduced to the minimum in the range of fundamental "Lock-in". The vortices develop in the immediate vicinity of the rear cylinder wall. The formation length varies linearly according to the recirculation bubble length. In the vicinity of the frequency fixing range, the cortices are powerful and of small size. This is indicated by a dense smoke and a minimal characteristic radius for the developed vortex.

Hot smoke is taken away by the vortices formed behind the cylinder. Its density is most important in the vortex formation zone. The maximum temperature along the wake center line is very sensitive to the cylinder deformation frequency. It characterizes the center of the developed vortex. This temperature is maximum in the vortex formation zone for all the deformation frequencies. The most important values of temperature are obtained for deformation frequencies close to the frequencies synchronization range (Lock-in).

The maximum rms for temperature fluctuation is recorded in the vortex formation zone. Its variation, with the deformation frequency, is significant, showing that the turbulence rate is more important for deformation frequencies which are in the vicinity of the synchronization range.

Hence, we conclude that the cylinder radial deformation can be used to control the cylinder wake. Following this work, we planning to carry out experiments for other flow modes to investigate the influence of this deformation for larger Reynolds numbers.

The experimental technique used in the present work is very simple to implement and requires no particular development except for the emissivity calculation of the tracer (smoke in this study). On the other hand, it presents some limitations which are summarized below:

The measurement is a surface measurement. The measurement is thus done only on the injection smoke plan and it is very difficult to perform tridimensional measurements.

The measurement capture frequency is 50 images per second. The Shannon theorem (Hlawatsch and Boudreaux-Bartels, 1992) (Mertins, 1992) stipulates that it would be impossible to detect phenomena which would occur at frequencies higher than 25 Hz.

The camera resolution for a distance of 1 m between the object and the camera is $3.89 \times 5.19$ mm$^2$. Eddies with lower dimensions than this resolution will not be distinguished and it would be very difficult to detect them with the camera.

The measured turbulence intensity is a total intensity. It is not possible to measure the turbulence intensity in a given direction. It will be assumed that turbulence is homogeneous.

## References


Armstrong, B.J., Barnes, F.H., Grant, I., 1986. The effect of a perturbation on the flow over a bluff cylinder. Phys. Fluids 29, 2095–2102.

Armstrong, B.J., Barnes, F.H., Grant, I., 1987. A comparison of the structure of the wake behind a circular cylinder in steady flow with that in a perturbed flow. Phys. Fluids 30, 19–26.

Barbi, C., Favier, D.P., Maresca, C.A., Telionis, D.P., 1986. Vortex shedding and lock-on of a circular cylinder in oscillatory flow. J. Fluid Mech. 170, 527–544.

Bearman, P.W., 1969. On vortex shedding from a circular cylinder in the critical Reynolds number region. J. Fluid Mech. 37, 577–587.

Blasius, H., 1908. Grenzchichten in Flussigkeiten mit Kleiner Reiburg. Z. Angew. Math Phys. Engl. Trans. NACA TM-1256 56, 1.

Carberry, J., Sheridan, J., Rockwell, D., 2003. Controlled oscillations of a cylinder: a new wake state. J. Fluids Struct. 17, 337–343.

Collins, W.M., Dennis, S.C.R., 1973. Flow past an impulsively started circular cylinder. Z. Angew, Math. Phys. Engl.Trans NACA TM-1256 56, 1.

Coutenceau, M., Bouard, R., 1977. Experimental determination of the main features of the viscous flow in the wake of a circular cylinder in uniform translation. Part-1, steady flow. J. Fluid Mech. 79, 231–256.

Gerrard, J.H., 1966. The mechanics of the formation region of the vortices behind bluff bodies. J. Fluid Mech. 25, 401–413.

Govardhan, R., Williamson, C.H.K., 2001. Mean and fluctuating velocity fields in the wake of a freely vibrating cylinder. J. Fluid Struct. 15, 489–501.

Green, R.B., Gerrard, J.H., 1993. Vorticity measurements in the near wake of a circular cylinder at low Reynolds numbers. J. Fluid Mech. 246, 675–691.

Griffin, O.M., 1995. A note on bluff body vortex formation. J. Fluid Mech. 284, 217–224.

Griffin, O.M., Ramberg, S.E., 1976. Vortex shedding from a cylinder vibrating in line with an incident uniform flow. J. Fluid Mech. 75, 526–537.

Griffin, O.M., Votaw, C.W., 1972. The vortex street in the Wake of vibrating cylinder. Appl. Mech. Rev. 51, 31–48.

Hall, S.E., Griffin, O.M., 1993. Vortex shedding and lock-on in a perturbed flow. ASME J. Fluids Eng. 115, 283–291.

Hanchi, S., 1998. Contribution à l'étude de l'écoulement et du transfert de chaleur autour d'un cylindre déformable. D. Phil. Thesis, University of Valenciennes and Hainaut-Cambresis.

Hlawatsch, F., Boudreaux-Bartels, G.F., 1992. Linear and quadratic time–frequency signal representations. IEEE Signal Process. Mag. 9 (2), 21–67.

Konstantinidis, E., Balabani, S., Yianneskis, M., 2003. effect of flow perturbations on the near wake characteristics of a circular cylinder. J. Fluid Struct 18, 367–386.

Koumoutsakos, P., Leonard, A., 1995. High-resolution simulations of the flow around the impulsively started cylinder using vortex method. J. Fluid Mech. 296, 1–38.

Kovasznay, L.S.G., 1970. The turbulent boundary layer. Ann. Rev. Fluid Mech. 2, 95–112.

Krishnamoorthy, S., Price, S.J., Paidoussis, M.P., 2001. Cross-flow past an oscillating circular cylinder: synchronization phenomena in the near wake. J. Fluid Struct. 15, 955–980.

Kundu, P.K., Cohen, I.M., 2002. Fluid Mechanics, second ed. Academic Press, Elsevier Science, USA, pp. 545–546.

Mertins, A., 1992. Signal Analysis: Wavelets, Filters Banks, Time–Frequency Transformations and Applications. John Wiley & Sons, pp. 221–230.

Ongoren, A., Rockwell, D., 1988. Flow structure from an oscillating cylinder. Part 2. Mode competition in the near wake. J. Fluid Mech. 191, 225–245.

Oualli, H., Hanchi, S., Bouabdallah, A., Askovic, R., 2004. Experimental investigation of the flow around a radially vibrating circular cylinder. J. Exp. Fluids 37 (6), 789–801.

Payne, R.B., 1958. Calculations of unsteady viscous flow past a circular cylinder. J. Fluid Mech. 4, 13.

Sarpkaya, T., 1979. Vortex induced oscillations. J. Appl. Mech. 46, 241–258.

Tanida, Y., Okajima, A., Watanabe, Y., 1973. Stability of a circular cylinder oscillating in uniform flow or in wake. J. Fluids Mech. 61, 769–784.

Ta Phuoc, L., 1980. Numerical analysis of unsteady secondary vortices generated by an impulsively started circular cylinder. J. Fluid Mech. 100 (1), 111–128.

Ta Phuoc, L., Bouard, R., 1985. Numerical solution of the early stage of the unsteady viscous flow around a circular cylinder: a comparison with experimental visualization and measurements. J. Fluid Mech. 160, 93–117.

Thom, A., 1933. The flux past circular cylinders at low speeds. Proc. R. Soc. Lond. A 141, 651.

Tomotika, S., Aoi, T., 1950. The steady flow of viscous fluid past a sphere and circular cylinders at small Reynolds numbers. Quart. J. Mech. Appl. Math. 3 (2), 140–161.

Zdravkovich, M.M., 1996. Different modes of vortex shedding: an overview. J. Fluid Struct. 10, 427–437.